Intensity and Polarization Self-Pulsations in VCSELs

Alessandro Scirè*[a], Josep Mulet[a], Claudio R. Mirasso[b] and Maxi San Miguel[a]

[a] Instituto Mediterráneo de Estudios Avanzados (IMEDEA), Consejo Superior de Investigaciones Científicas-Universitat de les Illes Balears, Campus Universitat Illes Balears, E-07071 Palma de Mallorca , Spain.

[b] Departament de Física, Universitat de les Illes Balears. E-07071 Palma de Mallorca, Spain.

ABSTRACT

We develop a model that describes the polarization dynamics of VCSELs with an absorbing region surrounding the active zone. We find that the dynamical behavior of the optical field is organized in four regions: stable linearly-polarized operation, intensity pulsations of a linearly-polarized component, pulsations of both total intensity and polarization, and polarization self-pulsations with constant total intensity. We characterize the four regions by computing the polarization resolved optical and power spectra. The predicted scenario agrees with recent experimental results.

1. INTRODUCTION

Edge-emitting lasers (EELs) with a narrow-stripe geometry may exhibit self-pulsations (SPs) due to the saturable absorber region surrounding the active zone.[1,2] This phenomenon has been implemented in clock extraction systems,[3] in synchronization schemes for encoded communication[4] and as a method to reduce the noise of laser diodes in optical disk systems.[5] Vertical-Cavity Surface-Emitting Lasers (VCSELs)[6] are important compact light sources for applications, e.g. in optical interconnects and optical data storage, due to their low threshold current, single-longitudinal mode operation and easy integrability in 2-D arrays. As in EELs, VCSELs may contain an unpumped region surrounding the central gain zone and therefore SPs conditions would be expected, especially in VCSELs with lateral confinement structures such as those with selective oxidization as well as proton implantation. Recently, SPs have been experimentally demonstrated in small radius, oxide confined VCSELs.[7,8] Since the polarization in VCSELs is not well stabilized,[9] the polarization properties of self-pulsating VCSELs is an interesting issue to be investigated.

In this contribution, we develop a model suitable to describe SPs in VCSELs operating in the fundamental transverse mode. The polarization dynamics is the new feature with respect to the well-known self-pulsing EELs. Our description of the absorbing region is similar to the one used in the Yamada's model.[1,2] Combining[10] the SFM and the Yamada approaches, we are able to investigate the polarization dynamics of VCSELs in presence of a saturable absorber. The paper is organized as follows, in Sec. 2 we present a detailed description of the model. In Sec. 3, we show the results of the linear stability analysis and we characterize the different dynamical regimes. Finally Sec. 4 is devoted to conclude and summarize our paper.

2. THE MODEL

We consider a VCSEL structure, as the one schematically shown in Fig. 1, where the central region (region 1) is the active zone, while the surrounding region in the radial direction (region 2) is the saturable absorber. These two regions are made from an identical crystal, but the current is only supplied in region 1. Since region 2 lacks of pumping, the electric field is adsorbed in this zone. The total intensity and polarization dynamics are described within the framework of the Spin-Flip Model[9,11] (SFM). Active and absorbing regions are treated as two four-level subsystems in which absorption and stimulated emission processes take place. The two subsystems are coupled through carrier diffusion processes and by the electric field profile. In the SFM the polarization state of the light

*Other author information: (Sent correspondence to M.S.M.): Email: maxi@imedea.uib.es; Telephone: +34-971-173229; Fax: +34-971-173426; URL: http//www.imedea.uib.es

is determined from the allowed transitions taking place in the active material: emission of a right (left) circularly-polarized photon corresponds to transitions in which the projection of the total material angular momentum $\vec{J}$ on the propagation direction changes by +1 (-1) in $\hbar$ units. Each of these two possible transitions imply the recombination of a spin-down (spin-up) electron-hole pair. Thus, it is natural to split the total carrier density in two different spin channels with opposite spin orientation ($\pm 1/2$). Finally, these two carrier reservoirs are directly coupled through spin-flip processes.[12] In addition to the spin dynamics in the active material, other effects such as the cavity anisotropies may lead to preference for a particular linear polarization. Combining the SFM and the Yamada approaches, we are able to investigate the polarization dynamics in a VCSEL in presence of a saturable absorbing region. A representation of the underlying physical mechanisms is sketched in Fig. 2. The equations governing the optical and material variables read

$$\frac{dE_\pm(t)}{dt} = \frac{1}{2}(1+i\alpha)\left[a_1\xi_1\left(N_1-N_{t1}\pm n_1\right)+a_2\xi_2\left(N_2-N_{t2}\pm n_2\right)-\kappa\right]E_\pm-(\gamma_a+i\gamma_p)E_\mp+\mathcal{G}_\pm(t)\,, \quad (1)$$

$$\frac{dN_1(t)}{dt} = \frac{J}{e}-\frac{N_1}{\tau_s}-\frac{N_1-vN_2}{T_{12}}-a_1\xi_1\left(N_1-N_{t1}+n_1\right)|E_+|^2-a_1\xi_1\left(N_1-N_{t1}-n_1\right)|E_-|^2\,, \quad (2)$$

$$\frac{dN_2(t)}{dt} = -\frac{N_2}{\tau_s}-\frac{N_2-N_1/v}{T_{21}}-a_2\xi_2\left(N_2-N_{t2}+n_2\right)|E_+|^2-a_2\xi_2\left(N_2-N_{t2}-n_2\right)|E_-|^2\,, \quad (3)$$

$$\frac{dn_1(t)}{dt} = -\gamma_s n_1-\frac{n_1-vn_2}{T_{12}}-a_1\xi_1\left(N_1-N_{t1}+n_1\right)|E_+|^2+a_1\xi_1\left(N_1-N_{t1}-n_1\right)|E_-|^2\,, \quad (4)$$

$$\frac{dn_2(t)}{dt} = -\gamma_s n_2-\frac{n_2-n_1/v}{T_{21}}-a_2\xi_2\left(N_2-N_{t2}+n_2\right)|E_+|^2+a_2\xi_2\left(N_2-N_{t2}-n_2\right)|E_-|^2\,, \quad (5)$$

where $E_\pm$ are the slowly-varying complex amplitudes of the two circularly-polarized components of the electric field, $N_{1,2}$ are the total carrier inversion between the conduction and valence bands, while $n_{1,2}$ are the differences of the carrier inversion with opposite spin orientations. The involved parameters have the following meaning (the suffix $i=1,2$ stands for the regions $1,2$): a_i is the differential gain, ξ_i is the fraction of optical power within the region i and can be calculated from a given transverse mode profile[13] $\Phi(\vec{r}_\perp)$

$$\xi_1 = \frac{\iint_{\text{region 1}}|\Phi(\vec{r}_\perp)|^2 d^2\vec{r}_\perp}{\iint_{-\infty}^{\infty}|\Phi(\vec{r}_\perp)|^2 d^2\vec{r}_\perp}\,, \quad (6)$$

and by normalization $\xi_2 = 1-\xi_1$. N_{ti} is the carrier density at transparency, κ is the cavity decay rate, τ_s is the electron lifetime due to spontaneous emission, T_{ij} is the typical electron diffusion time from region i to region j, v is the ratio of the two regions volume: $v \equiv V_1/V_2 \approx T_{12}/T_{21}$, γ_s is the spin flip rate, γ_a and γ_p are the amplitude (dichroism) and phase (birefringence) anisotropies respectively. The linewidth enhancement factor α describes the

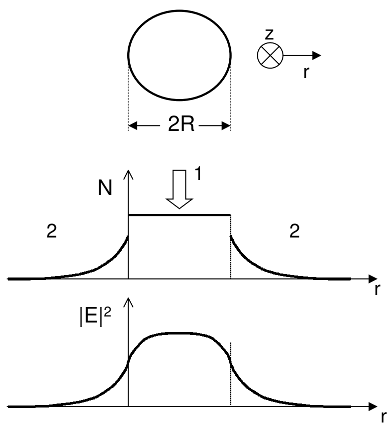

Figure 1. Schematic representation of a VCSEL structure with saturable absorber. The center region is the active region (region 1) and the surrounding region in the radial direction is the absorbing region (region 2). Electron distribution is uniform in region 1 and is proportional to the optical power distribution in region 2.

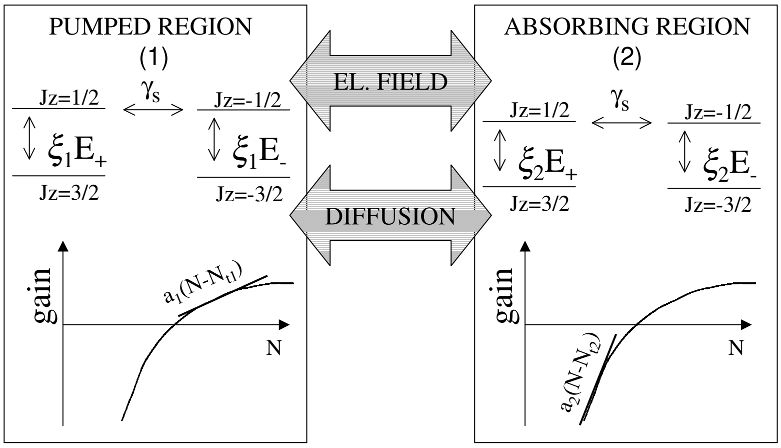

Figure 2. Description of the polarization in self-pulsating VCSELs: Two coupled four-level systems are obtained combining the Yamada and SFM models. The carrier dependence of the gain is approximated by a linear dependence (with different slopes) in the two regions.

phase amplitude coupling. It is well known that the relation between the gain coefficient and the carrier density is nonlinear. We approximate the carrier dependence of the gain function [Fig.2] by a linear approximation around each operating points. Thus, we take different values of a_1 and a_2 and N_{t1} and N_{t2}, whether the region 1 or 2 is considered. Finally, spontaneous emission processes are accounted through two independent Langevin noise sources $\mathcal{G}_{\pm}(t)$.

2.1. Dimensionless model

For the sake of simplicity and numerical purposes, we rescale the dynamical variables in Eqs. (1)-(5) by

$$F_{\pm} = \sqrt{\tau_1 a_1 \xi_1}\, E_{\pm}\,,$$
$$D_i = \frac{a_i \xi_i}{\kappa}\,(N_i - N_{ti})\,, \qquad d_i = \frac{a_i \xi_i}{\kappa} n_i\,.$$

With the new variables, the equations (1)-(5) reduce to

$$\dot{F}_{\pm}(t) = \frac{1}{2}(1+i\alpha)\,[D_1 + D_2 \pm d_1 \pm d_2 - 1]\,F_{\pm} - (\varepsilon_a + i\varepsilon_p)F_{\mp} + f_{\pm}(t)\,, \tag{7}$$
$$\dot{D}_1(t) = \gamma_1\left[\mu_1 - D_1 - (D_1+d_1)|F_+|^2 - (D_1-d_1)|F_-|^2 + c_{12}D_2\right]\,, \tag{8}$$
$$\dot{D}_2(t) = \gamma_2\left[\mu_2 - D_2 - a(D_2+d_2)|F_+|^2 - a(D_2-d_2)|F_-|^2 + c_{21}D_1\right]\,, \tag{9}$$
$$\dot{d}_1(t) = -\gamma_{s1}d_1 - \gamma_1\left[(D_1+d_1)|F_+|^2 - (D_1-d_1)|F_-|^2 - c_{12}d_2\right]\,, \tag{10}$$
$$\dot{d}_2(t) = -\gamma_{s2}d_2 - \gamma_2\left[a(D_2+d_2)|F_+|^2 - a(D_2-d_2)|F_-|^2 - c_{21}d_1\right]\,, \tag{11}$$

where the subindexes $1, 2$ stand for the pumped and absorbing region, respectively. The equations are written in a dimensionless form such that the time t is measured in κ units. The dot acting onto the dynamical variables means derivative with respect to the dimensionless time. We have also introduced the following dimensionless parameters

$$\tau_i = \frac{\tau_s T_{ij}}{\tau_s + T_{ij}}\,, \qquad \gamma_i = \frac{1}{\tau_i \kappa}\,, \tag{12}$$
$$\tau_{si} = \frac{T_{ij}}{\gamma_s T_{ij} + 1}\,, \qquad \gamma_{si} = \frac{1}{\tau_{si}\kappa}\,, \qquad c_{ij} = \frac{\tau_i a_i \xi_i}{T_{ij} a_j \xi_j}\,, \tag{13}$$
$$\mu_i = \frac{\tau_i a_i \xi_i}{\kappa}\left[\delta_{i1}\frac{J}{e} - \frac{N_{ti}}{\tau_i} + \frac{N_{ti}}{T_{ij}}\right]\,, \tag{14}$$
$$a = \frac{\tau_2 a_2 \xi_2}{\tau_1 a_1 \xi_1}\,, \qquad \varepsilon_a = \gamma_a/\kappa\,, \qquad \varepsilon_p = \gamma_p/\kappa\,, \tag{15}$$

where $i = 1, 2$ and $j = 3-i$, δ_{i1} is the Kronecker symbol. The effective injection currents, with respect to transparency, are μ_1 and μ_2. Since the current is only supplied in the central region, $\mu_1 > 0$ while $\mu_2 < 0$. Carrier diffusion is still present in the equations through the coupling terms $c_{12}D_1$ and $c_{21}D_2$. The Langevin noise sources[17] $f_\pm(t)$ can be approximated by

$$f_\pm(t) = \sqrt{\beta\xi_1\,\gamma_1(D_1 \pm d_1) + \beta\xi_2\,\gamma_2(D_2 \pm d_2)}\,\zeta_\pm(t)\,, \tag{16}$$

where $\beta\xi_i$ represents the fraction of the spontaneously emitted photons that goes into the zone i of the lasing mode, $\zeta_\pm$ are two independent complex Gaussian random numbers, with zero mean $\langle\zeta_\pm(t)\rangle = 0$ and correlation $\langle\zeta_\pm(t)\zeta^*_\pm(t')\rangle = 2\delta(t-t')$.

3. RESULTS

In this section we start analyzing the linearly polarized steady-state solutions of our model. We also discuss the effect of the saturable absorber onto the threshold condition. Next, we perform the linear stability analysis (LSA) of the linearly-polarized solutions. Finally, we describe the significative dynamical regions of a VCSEL with saturable absorber by the help of spectral measurements and by analyzing the Stokes parameters.

3.1. Steady states. Threshold condition.

We start our discussion looking at the linearly polarized (LP) steady state solutions of Eqs. (7)-(11). The electrical fields is expressed as $F_\pm(t) = Qe^{i(\omega_\pm t \pm \varphi)}$, and the time derivatives of the carrier densities are set to zero. We find two types of LP solutions: $\varphi = 0$ along the x-axis and $\varphi = \pi/2$ along the orthogonal direction. Since we observed that our results are only weakly dependent on ε_a, we take for simplicity $\varepsilon_a = 0$ in the rest of the paper. In this limit, $\omega_\pm = -\varepsilon_p$ for a x-LP solution and $\omega_\pm = \varepsilon_p$ for a y-LP solution. The total carrier inversions are in turn given by

$$\bar{D}_1 = \frac{\mu_1(1+aA) + \mu_2 c_{12}}{(1+A)(1+aA) - c_{12}c_{21}}\,, \tag{17}$$

$$\bar{D}_2 = \frac{\mu_2(1+A) + \mu_1 c_{21}}{(1+A)(1+aA) - c_{12}c_{21}}\,. \tag{18}$$

The difference of the carrier inversion $\bar{d}_i = 0$ in LP states. The total intensity $A \equiv 2Q^2$ satisfies the gain clamping condition $\bar{D}_1 \pm \bar{d}_1 + \bar{D}_2 \pm \bar{d}_2 = 1$, leading to a quadratic equation for A that reads

$$aA^2 + [a(1-\mu_2) + (1-\mu_1)]A + 1 - \mu_1(1+c_{21}) - \mu_2(1+c_{12}) - c_{12}c_{21} = 0\,. \tag{19}$$

For our choice of parameters, Eq.(19) has only one positive root. The laser threshold is modified due to the presence of the absorber, and is defined[2] as the circumstance for which the trivial solution $A = 0$ loses stability in absence of spontaneous emission. By setting $A = 0$ in Eqs. (17)-(18) and imposing the gain clamping condition we find the threshold current

$$\mu_{1th} = \frac{1 - c_{12}c_{21} - \mu_2(c_{12}+1)}{1 + c_{21}}\,. \tag{20}$$

It is worth noting that when the optical mode is well confined within the region one, i.e. $\xi_1 \approx 1$ and $\xi_2 \approx 0$, Eq. (20) reduces to $\mu^{sol}_{1th} = 1$, which is the case of VCSELs without absorbing region. We also find an interpretation of the different terms in Eq. (20); there is an increase in threshold current due to the absorption ($\mu_2 < 0$) and due to the carrier diffusion from region 1 to region 2 (c_{12}), while the threshold decreases if the inverse carrier flux is favored (c_{21}).

3.2. Linear stability analysis

A linear stability analysis[9] of the two LP solutions of the system (7)-(11) can be carried out by introducing a small perturbation to the LP steady state solutions

$$\begin{aligned} F_{\pm}(t) &= (Q + a_{\pm}(t))\, e^{i(\omega_{\pm} t \pm \varphi)}\,, && (21)\\ D_{1,2}(t) &= \bar{D}_{1,2} + \Delta_{1,2}(t)\,, && (22)\\ d_{1,2}(t) &= \delta_{1,2}(t)\,, && (23) \end{aligned}$$

where $a_{\pm}$ is a complex perturbation of the field amplitude, Δ_i and δ_i $(i = 1, 2)$ are real perturbations to the carrier variables. Upon substituting the perturbed solutions (21)-(23) in the equations of the model (7)-(11) and linearizing to first order in perturbations, we obtain a set of coupled linear differential equations for $a_{\pm}$, Δ_i and δ_i which, written for the variables $S \equiv a_+ + a_-$ and $R \equiv a_+ - a_-$ decouples into two subsets, one (4×4) that accounts for the stability of the total intensity, and one (4×4) that describes the polarization stability. The total intensity subset reads

$$\begin{aligned} \dot{S}(t) &= (1 + i\alpha) Q(\Delta_1 + \Delta_2)\,, && (24)\\ \dot{S}^*(t) &= (1 - i\alpha) Q(\Delta_1 + \Delta_2)\,, && (25)\\ \dot{\Delta}_1(t) &= -\gamma_1 Q \bar{D}_1 (S + S^*) - \gamma_1 (1 + 2Q^2)\Delta_1 + \gamma_1 c_{12} \Delta_2\,, && (26)\\ \dot{\Delta}_2(t) &= -a\gamma_2 Q \bar{D}_2 (S + S^*) - \gamma_2 (1 + 2aQ^2)\Delta_2 + \gamma_2 c_{21} \Delta_1\,, && (27) \end{aligned}$$

which determines the stability of an arbitrary linearly-polarized solution. A general solution of Eqs. (24)-(27) can be expressed by

$$\begin{pmatrix} S(t) \\ S^*(t) \\ \Delta_1(t) \\ \Delta_2(t) \end{pmatrix} = \begin{pmatrix} S(0) \\ S^*(0) \\ \Delta_1(0) \\ \Delta_2(0) \end{pmatrix} e^{st}\,. \qquad (28)$$

Due to the arbitrariness in a global phase,[11] the actual dimension of the total intensity subset is three, resulting in a third-order characteristic polynomial for s

$$s^3 + C_1 s^2 + C_2 s + C_3 = 0 \qquad (29)$$

where

$$\begin{aligned} C_1 &= \gamma_1 (1 + A) + \gamma_2 (1 + aA)\,, && (30)\\ C_2 &= \frac{1}{2}\left[\gamma_1 \bar{D}_1 + a\gamma_2 \bar{D}_2\right] A + o(\gamma_1\gamma_2)\,, && (31)\\ C_3 &= \frac{1}{2}\gamma_1\gamma_2 A \left[(1 + aA)\bar{D}_1 + (1 + A)\bar{D}_2 + ac_{12}\bar{D}_2 + c_{21}\bar{D}_1\right]\,. && (32) \end{aligned}$$

As the carrier decay rates[14] $\gamma_1 \sim \gamma_2$ are typically $o(10^{-3})$, a simplified analysis can be performed. Applying the Routh-Hurwitz criteria,[15] and neglecting $o(\gamma_i^2)$ terms, we obtain the boundary stability conditions that read

$$\mu_1 + a_2\mu_2\Gamma^2 + (a_2\Gamma - 1)\left[(c_{21}\Gamma + c_{12})\,\bar{D}_1 - c_{12}\right] = 0\,, \qquad (33)$$

$$\Omega^2 = \frac{1}{2}\left[\gamma_1 \bar{D}_1 + a_2\gamma_2 \bar{D}_2\right] A > 0\,, \qquad (34)$$

with $\Gamma \equiv \gamma_2/\gamma_1$. When Eq. (33) is fulfilled, the total intensity loses its stability through a Hopf bifurcation, giving rise to pulsations at frequency Ω. More generally, in the region bounded by the laser threshold (20) and the Hopf bifurcation limit (33), the total intensity exhibits a pulsating dynamic.

The polarization stability decouples (in the linear approximation) to the total intensity stability, and is described by the second linear subset

$$\begin{aligned} \dot{R}(t) &= (1 + i\alpha) Q(\delta_1 + \delta_2) \pm 2(\varepsilon_a + i\varepsilon_p) R && (35)\\ \dot{R}^*(t) &= (1 - i\alpha) Q(\delta_1 + \delta_2) \pm 2(\varepsilon_a + i\varepsilon_p) R^* && (36)\\ \dot{\delta}_1(t) &= -\gamma_1 Q \bar{D}_1 (R + R^*) - (\gamma_{s1} + 2\gamma_1 Q^2)\delta_1 + \gamma_1 c_{12}\delta_2 && (37)\\ \dot{\delta}_2(t) &= -a\gamma_2 Q \bar{D}_2 (R + R^*) - (\gamma_{s2} + 2\gamma_2 a Q^2)\delta_2 + \gamma_2 c_{21}\delta_1 && (38) \end{aligned}$$

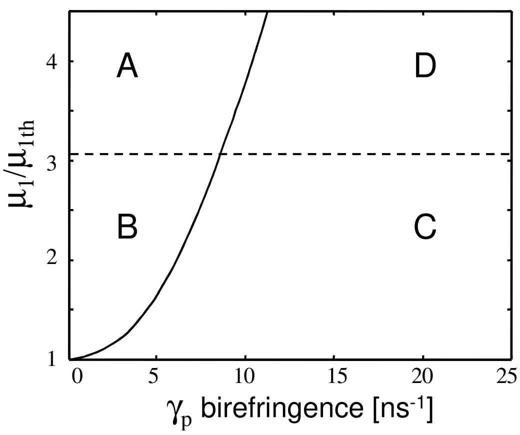

Figure 3. Phase diagram (μ_1/μ_{1th} vs $\gamma_p = \varepsilon_p \kappa$) for the stability of the linearly polarized solutions. The four regions are A) y-LP stable, B) pulsations in one polarization, C) coupled pulsations and D) polarization pulsations. The numerical study has been performed with the following choice of parameters: $\mu_2 = -32$, $\gamma_1 = 1.09 \times 10^{-3}$, $\gamma_2 = 1.13 \times 10^{-3}$, $\alpha = 3$, $\kappa = 390$ ns^{-1}, $c_{12} = 2.84 \times 10^{-2}$, $c_{21} = 1.91$, $\gamma_{s1} = 0.25$, $\gamma_{s2} = 0.25$, $a_2 = 8.7$.

where the $\pm$ signs stand for the stability of a $x-$LP solution and $y-$LP solution, respectively. As already known for the case of a VCSEL without absorber,[11] that the cavity anisotropies play an important role in the polarization stability. They are accounted for in the model through the parameters ε_a and ε_p. In our case, there is a novelty that comes from the spin dynamics $\delta_{1,2}$ taking place in both regions, which are directly coupled through diffusion processes. The dimension of the polarization subset (35)-(38) is four and an analytical approach is quite involved. Next, we explain how to obtain the polarization stability through semi-analytical methods.

3.3. Operation regimes.

We numerically find the stability of the polarization by solving the characteristic equation emerging from the polarization subset (35)-(38). In the phase diagram μ_1/μ_{1th} vs. the birefringence $\gamma_p \equiv \varepsilon_p \kappa$ [Fig. 3], we represent the stability boundaries, i.e., the situation where at least one eigenvalue becomes imaginary pure, while the other ones have negative real part. We distinguish four different regions when looking to the eigenvalues of the total intensity and polarization subsets.

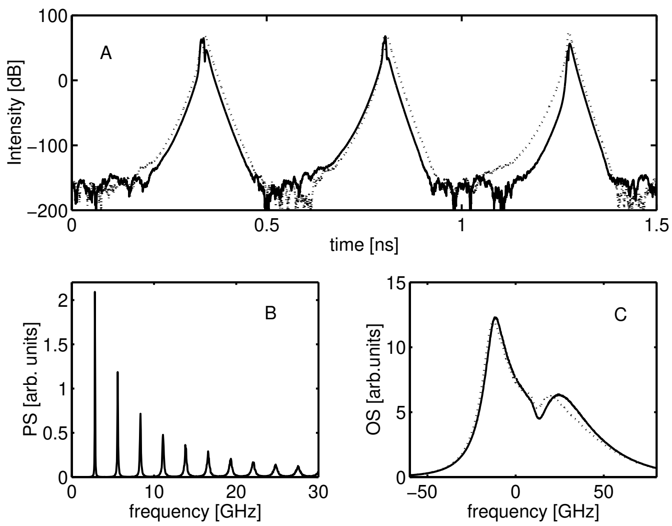

Figure 4. A) time traces x-LP (dotted), y-LP (solid) in region C of figure 1, ($\mu_1/\mu_{1th} = 2$, $\gamma_p = 20$ ns^{-1}), B) total intensity power spectrum, C) polarization resolved optical spectra for x-LP (dotted) and y-LP (solid).

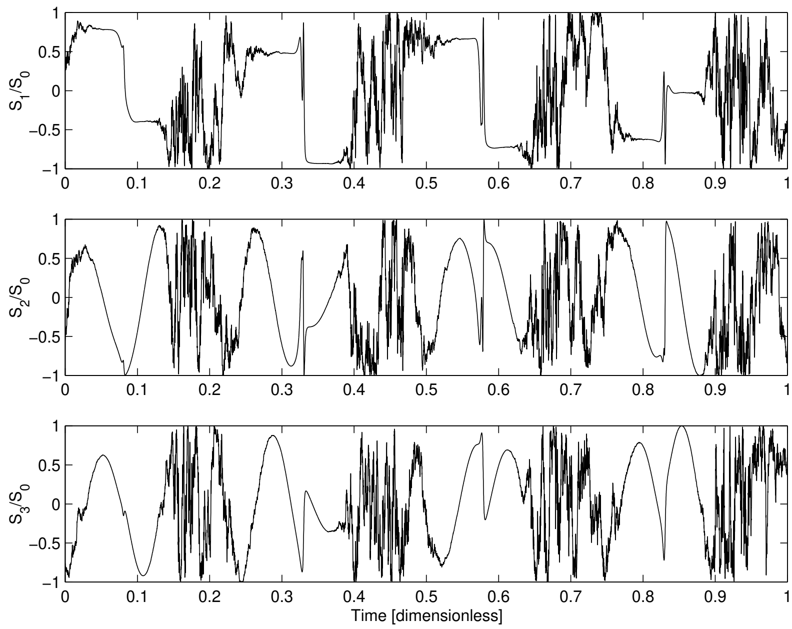

Figure 5. Time traces of the Stokes parameters in region C. The parameters are the same as in Fig. 4.

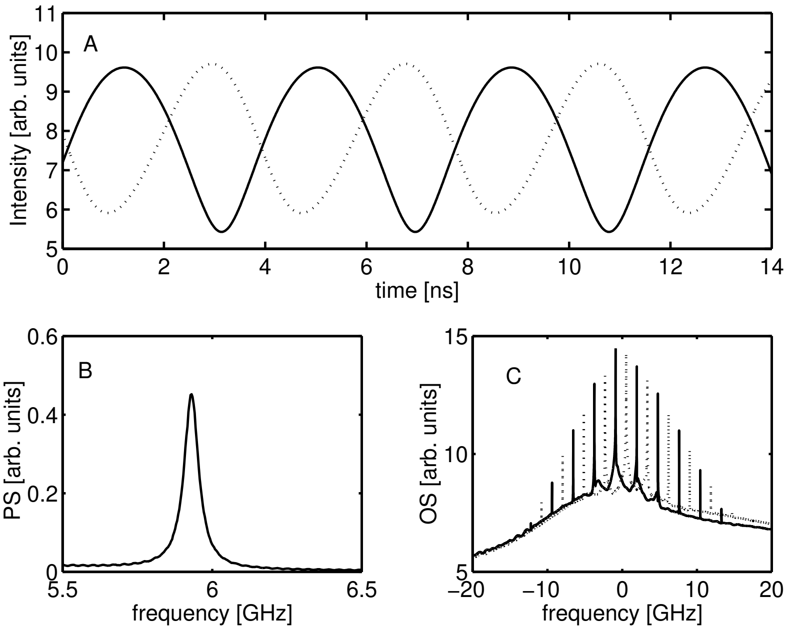

Figure 6. A) time traces x-LP dotted, y-LP solid in region D of figure 1, ($\mu_1/\mu_{1th} = 4$, $\gamma_p = 20$ ns^{-1}), B) total intensity power spectrum, C) polarization resolved optical spectra for x-LP (dotted) and y-LP (solid).

In the region A only the y-LP solution is stable and the system reaches steady-state operation in such a polarization. In the region B, we observe total intensity pulsations in a well defined polarization orientation. In the latter, the pumping process is able to excite the carriers to sufficiently high levels, and consequently the field intensity increases as soon as the unsaturated gain overcome the losses, originating the onset of a pulse. This situation occurs when the condition (20) is satisfied. In addition, the large increase in intensity saturates the absorber, that in turn, leads to a larger output powers and subsequently to a saturation of the gain in the active zone. This last mechanism produces a decay of the electric field to the noise level. The self-sustained repetition of this process produces a regular train of pulses. This mechanism is typical in many laser structures that include a saturable absorber. For this reason, the time traces we obtain in region B are quite similar to those of SPs in EELs when polarization degrees of freedom are disregarded.

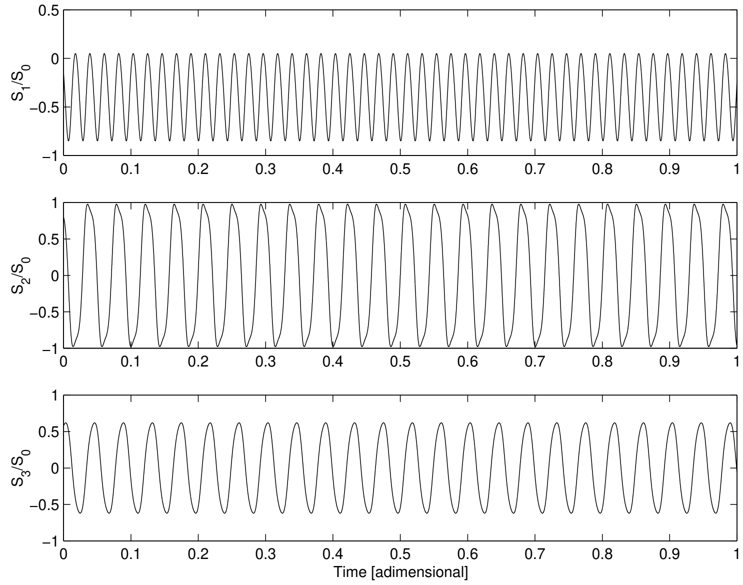

Figure 7. Time traces of the stokes parameters in region D (Polarization Pulsations). The parameters are the same that in Fig. 6.

In the region C both total intensity and polarization subsets are linearly unstable. The time traces of the two linear polarizations components in region C [see Fig. 4(A)] display amplitude modulation (AM) with the shape of strong pulses. The shape and the height of each pulse, as well as the time position change from pulse to pulse. The spontaneous emission noise has been demonstrated to cause time jitter of the pulses,[16] while the irregularities of the height and shape of the pulses seems to be a peculiarity of the involved phase and polarization dynamics present in region C. We call this regime as *Coupled Pulsations* (CP) of the polarization and total intensity. In order to better characterize the underlying dynamics, we compute the power spectra of the total intensity

$$PS(\omega) \equiv \left\langle \left| \int_{-\infty}^{\infty} \delta P(t) e^{-i\omega t} dt \right|^2 \right\rangle , \tag{39}$$

and the optical spectra of the linear polarization components

$$OS_{x,y}(\omega) \equiv \left\langle \left| \int_{-\infty}^{\infty} F_{x,y}(t) e^{-i\omega t} dt \right|^2 \right\rangle , \tag{40}$$

with $P(t) \equiv |F_x|^2 + |F_y|^2$, $\delta P(t) = P(t) - \bar{P}$, and $\langle \cdot \rangle$ means average over different noise realizations. The power spectrum [Fig. 4(B)] shows a fundamental frequency (corresponding to Eq. (34) near the bifurcation) and harmonics. In addition to the AM, the two components undergo strong phase modulation (PM). The polarization resolved optical spectra [Fig. 4(C)] show an asymmetric double-peaked profile, typical of a gain switched semiconductor laser,[18] in both polarizations. The ratio between the width of the total optical spectrum [Fig. 4(C)], which represents the averaged phase-sweep during each pulse, and the fundamental peak position, is ~ 40 being of the same order of the experimentally reported value.[7] Each polarization is pulsating, but the relative phase between the two polarizations changes in a complicated way during the pulse, leading to irregularities in the height and shape of the resulting total intensity pulse. Figure 5 shows the time traces of the Stokes parameters[17] in region C. During the intra-pulse intervals, the Stokes parameters strongly fluctuate since the optical power reaches the noise level. When the pulse grows from the noise level, the strong amplitude modulation is coupled in a strongly non-linear way to the relative phase between F_+ and F_- and to the ellipticity of the outgoing field through a combined effect of the α- factor and birefringence. This final result manifests itself in a highly complex dynamics in the Poincaré sphere, while the pulse takes place.

When moving from region C to D the fundamental frequency increases until the locus Eq. (33) is crossed, afterward a different dynamical regime arises. Above the absorber saturation locus (33), the VCSEL can emit CW and no longer in a pulsating total intensity, since the pump level is high enough to make transparent the absorbing region. Since for our parameters choice the VCSEL without absorber ($\mu_2 = c_{12} = c_{21} = 0$) would emit in one defined polarization, we find that the effect of the absorber is to destabilize the polarization in region D. The time traces [Fig. 6(A)] show a nearly out-of-phase AM composed by harmonic pulsations in the two polarization components. Since the two LP-solutions are both unstable, the system shows a time dependent solution that allows the total intensity to be nearly constant. We call this regime *polarization pulsation* (PP). The power spectrum [Fig. 6(B)] shows a single peak at twice the PP frequency. The residual total intensity modulation is due to non-linear coupling between the total intensity and polarization dynamics: the two subsets (24)-(27) and (35)-(38) describe the total intensity and polarization stability if the two problems were independent, but this is true only in the linear approximation. In the complete system (7)-(11) the total intensity and the polarization are coupled by non-linear terms. Therefore a small ripple in the total intensity can be observed. A harmonic PM is also present, in both polarizations, as shown in the polarization resolved OS [Fig. 6(A)]. We remark that, on the contrary to the transition from A to B, the transition form C to D is not sharp. The strong pulses smoothen to a chaotic attractor which involves both polarization and total intensity. The attracting region get smaller until the chaotic attractor transforms into a limit cycle in the Poincaré sphere, surrounding the $\hat{y}$-LP fixed point, as shown in Fig.7. In the experiments,[7] a similar transition from strongly chirped pulses to harmonic pulsations was also found when increasing the pump. Our results in region C and D are in agreement with the experimentally measured power and optical spectra.

4. CONCLUSIONS

We have demonstrated that polarization self-pulsations in VCSELs are possible under certain operation conditions. As a result of analytical and numerical analysis of our model, we have found regions of stable operation, coupled pulsations of the polarization and the total intensity, and polarization self-pulsations at nearly constant total intensity. These regions that appear when changing the injection current compare successfully with the experimental results. More generally, we conclude that our model constitutes an adequate framework to study self-pulsations in vertical-cavity surface-emitting lasers when polarization degrees of freedom are involved.

Acknowledgements

This work has been funded by the European Commission through the VISTA HP-TRN, Marie Curie IF MCFI-2000-00617, OCCULT project, IST-2000-29683 and the Spanish MCyT under projects TIC99-0645-C05-02, BFM 2000-1108, MCyT SINFIBIOS BFM 2001-0341-C02-01.

REFERENCES

1. C. R. Mirasso, G. H. M. van Tartwijk, E. Hernández-García, D. Lenstra, S. Lynch, P. Landais, P. Phelan, J. O' Gorman, M. San Miguel and W. Elsässer, "Self-Pulsating Semiconductor Lasers: Theory and Experiment," *IEEE J. Quantum Electron.*, vol. 35, p. 764, 1999.
2. M. Yamada, " A Theoretical Analysis of Self-Sustained Pulsation Phenomena in Narrow-Stripe Semiconductor Lasers," *IEEE J. Quantum Electron.* vol. 29, p. 1330, 1993.
3. P. Rees, P. McEvoy, A. Valle, J. O'Gorman, S. Lynch, P. Landais, L. Pesquera and J. Hegarty, " A Theoretical Analysis of Optical Clock Extraction Using a Self-Pulsationg Laser Diode," *IEEE J. Quantum Electron.* vol. 35, p. 221, 1999.
4. C. Juang, T. M. Hwang, J. Juang, L. Wen-Wei, "A synchronization scheme using self-pulsationg laser diodes in optical chaotic communications," *IEEE J. Quantum Electron.* vol. 36, p. 300, 2000.
5. M. Yamada and T. Higashi, "Mechanism of the noise reduction method by superposition of high frequency current for semiconductor injection lasers," *IEEE J. Quantum Electron.* vol. 29, p. 1330, 1993.

6. K. B. Ebeling in *Semiconductor Quantum Optoelectronics*, edited by A. Miller, M.Ebrahimzadeh and D.M. Finlaynson (Institute of Physics, Bristol, 1999), p.339.
7. M. B. Willemsen, A. S. van de Nes, M. P. van Exter,J. P. Woerdman, M. Brunner and R. Hovel, “Self-pulsations in vertical-cavity semiconductor lasers,” *Appl. Phys. Lett.*, vol. 77, p. 3514, 2000.
8. J. A. Hudgings, R. J. Stone, C. Chang, S. F. Lim, K. Y. Lau and C. J. Chang-Hasnain “Dynamic behavior and applications of a three-contact vertical-cavity surface-emitting laser,”*IEEE J. Quantum Electron.* vol. 5, p. 512, 1999.
9. M. San Miguel, Q. Feng and J. V. Moloney, “Light-polarization dynamics in surface-emitting semiconductor lasers,” *Phys.Rev. A*, vol. 52, p. 1728, (1995).
10. A. Scirè, J. Mulet, C. R. Mirasso, and M. San Miguel. “Total intensity and polarization self-pulsations in VCSELs,” to appear in *Opt. Lett.*, (2002).
11. J. M. Regalado, F. Prati, M. San Miguel and N. B. Abraham, “Polarization properties of vertical-cavity surface-emitting lasers,” *IEEE J. Quantum Electron.* vol. 33, p. 765, 1997.
12. L.Viña, “Spin relaxation rate in low-dimensional systems,” *J. Phys.: Condens. Matter* vol. 11, p. 5929, 1999.
13. J. Mulet and S. Balle. To appear in *IEEE J. of Quantum Electron.* 2002.
14. T. W. Carr and T. Erneux, “Dimensionless rate equations and simple conditions for self-pulsing in laser diodes,” *IEEE J. Quantum Electron.* vol. 37, p. 1171, 2001.
15. G. A. Korn and T. M. Korn, *Mathematical Handbook for Scientist and Engineers*, Mc Graw-Hill, NY (1968).
16. G. H. M. van Tartwijk and M. San Miguel, “Optical feedback on self-pulsating semiconductor lasers,” *IEEE J. Quantum Electron.* vol. 32, p. 1191, 1996.
17. J. Mulet, C. R. Mirasso and M. San Miguel, “Polarization resolved intensity noise in vertical-cavity surface -emitting lasers,” Phys. Rev. A, vol. 64, p. 023817, 2001.
18. See for instance G. P. Agrawal, N. K. Dutta, *Long wavelength semiconductor lasers*, Van Nostrand, NY (1986), p.265.